Superconductor bearings, flywheels and transportation

2012 Supercond. Sci. Technol. 25 014007

(http://iopscience.iop.org/0953-2048/25/1/014007)

Supercond. Sci. Technol. **25** (2012) 014007 (16pp) doi:10.1088/0953-2048/25/1/014007

Superconductor bearings, flywheels and transportation

F N Werfel, U Floegel-Delor, R Rothfeld, T Riedel, B Goebel, D Wippich and P Schirrmeister

Adelwitz Technologiezentrum GmbH (ATZ), Rittergut Adelwitz 16, D-04886 Arzberg-Adelwitz, Germany

E-mail: werfel@t-online.de

Received 7 September 2011, in final form 6 October 2011
Published 1 December 2011
Online at stacks.iop.org/SUST/25/014007

Abstract

This paper describes the present status of high temperature superconductors (HTS) and of bulk superconducting magnet devices, their use in bearings, in flywheel energy storage systems (FESS) and linear transport magnetic levitation (Maglev) systems. We report and review the concepts of multi-seeded REBCO bulk superconductor fabrication. The multi-grain bulks increase the averaged trapped magnetic flux density up to 40% compared to single-grain assembly in large-scale applications. HTS magnetic bearings with permanent magnet (PM) excitation were studied and scaled up to maximum forces of 10 kN axially and 4.5 kN radially. We examine the technology of the high-gradient magnetic bearing concept and verify it experimentally. A large HTS bearing is tested for stabilizing a 600 kg rotor of a 5 kWh/250 kW flywheel system. The flywheel rotor tests show the requirement for additional damping. Our compact flywheel system is compared with similar HTS–FESS projects. A small-scale compact YBCO bearing with *in situ* Stirling cryocooler is constructed and investigated for mobile applications. Next we show a successfully developed modular linear Maglev system for magnetic train operation. Each module levitates $0.25t$ at 10 mm distance during one-day operation without refilling LN_2. More than 30 vacuum cryostats containing multi-seeded YBCO blocks are fabricated and are tested now in Germany, China and Brazil.

(Some figures may appear in colour only in the online journal)

1. Introduction

The performance of melt-textured high-T_c superconducting bulks has the significant potential of magnetic-force-based applications. For up-scaling the magnetic forces both the HTS bulk properties and availability of large bulks were coming into the focus. The successful laboratory fabrication of YBCO and REBCO (RE = Sm, Dy, Gd and Nd) single-grain bulk material is well understood in the last decade [1–6] whereby YBCO is the 'working horse'. SmBCO, GdBCO and NdBCO often grew under reduced oxygen atmosphere and the fine-tuned temperature profile shows even better magnetic properties at large crystals [7]. In parallel, efficiency attempts both in a low-cost fabrication [8] as well as to improve the seeding technology [9] have been recently shown.

The ATZ Company has studied the efficient and economic production of melt-textured bulk high T_c materials, starting with polycrystalline materials [3]. The random grain orientation was replaced by single-grain melt texturing and larger bulks by multi-seed technology. The HTS in-house production is strictly application-oriented and the engineering application covers a number of interdisciplinary fields. With the HTS bulk material we have successfully developed high-T_c superconducting magnetic devices for prototyping power energy application and magnetic levitation machinery.

Like HTS materials, magnetic bearings have been described extensively [10–13]. The principal benefit of superconducting magnetic bearings (SMB) stems from low-drag torque and the self-centering, unlubricated, wear-free and vacuum-compatible operation. In particular, radial-type HTS bearings are compact and robust in design, suitable for supporting high loads. In addition, axial HTS bearings are developed as well as a levitation demonstrator people-loading platform and bottom flywheel magnetic bearing. However, in contrast to ball bearings, SMB are an integral part of the overall design and cannot be specified in terms of simple mechanical

interfaces. Control of the SMB properties such as levitation pressure (load), restoring forces (stiffness) and damping could be of special importance in the desired applications. Therefore, before the large bearing projects were conceptualized, the basic parameters like force, stiffness, damping and creep were studied.

Journal-type magnetic bearing design and improved HTS bulk material properties increasingly fulfill the requirements of robust and reliable technical applications. The present status is characterized by maximum load up to 1.2 ton, stiffnesses at the 3–4 kN mm^{-1} level and simultaneous self-stabilization in axial and radial directions. Some applications with encapsulated bulk HTS require large gap operation of 5–6 mm and reliable machine cooling in the 50–60 K regions. We will give here design and handling instructions for the fabrication of HTS magnetic bearings.

A decade before, the HTS bearing design effort was focused on the passive magnetic stabilization of small and medium weighted rotors demonstrating safe operation in a centrifuge, laser scanner and wafer carrier [14–16]. As the rotational systems increase in size, it becomes a significant challenge to provide full magnetic suspension for up to 1000 kg loads.

For this purpose several 200 mm HTS bearings of 10 kN load capacity were tested and fabricated and finally integrated in a 5 kWh/250 kW flywheel energy storage system. The enhancement of the magnetic flux density is a physical key for increasing the present 10 N cm^{-2} bearing force density up to tenfold in the future with coils instead of PMs.

The objectives of this paper are to discuss the present status of high load superconducting passive magnetic bearings suspending technical wheels and, in particular, to describe the progress in design, development and safe operation.

A corresponding effort in designing and testing HTS bearings to suspend and rotate demonstrators of energy storage flywheels is reviewed [16–18]. The device efficiency depends on the overall storage design and the dynamical properties, e.g. the practical maximum rim speed obtainable rather than the individual bearing parameters.

From the basic concepts the rotors are suspended by superconducting thrust bearings in the bottom and/or top position interacting axially with permanent magnets. Alternatively, an HTS bearing can be designed in radial geometry. The HTS magnet stator is usually an array of some tens of glued small single-grain YBCO blocks. This axial geometry is easier to handle: however, it limits an up-scaling of bearing forces due to the need to increase the diameter of the PM rotor and HTS stator. A growing lateral bearing extension is unfavorable for the rotor speed and stability (centrifugal forces). We compare in section 3.5 the different concepts of magnetic flywheel stabilization and propose an outlook for future development.

Linear magnetic levitation of small trains attracted a great deal of interest shortly after the discovery of HTS. However it took about 15 yr to develop the first man-loading system [19]. Further real-scale-sized magnetic levitation (Maglev) systems followed [20, 21], mostly operating along short distances of a few meters on a double PM track. The optimum magnetic rail configuration is reviewed and compared [22–25]. The greatest disadvantage and simultaneous technical challenge was the cooling of the bulk HTS in open vessels with Styrofoam insulation.

For mobile applications in levitated trains or demonstrator magnets we examine the performance of on-board cryogenics either by LN_2 or a cryocooler. The mechanical, electrical and thermodynamical requirements of compact vacuum cryostats for Maglev train operation were studied systematically. More than 30 units are manufactured and tested. The load-to-weight ratio is more than 10 and favors group module device constructions up to 5*t* load on a permanent magnet track. A linear Maglev transport system consisting of four modular cryostat units has recently been fabricated in a prototyping process. The four HTS cryostats can carry almost 1 ton at 10–12 mm magnetic gap above a magnetic guideway with a force density of about 5 N cm^{-2}. Due to perfect thermal insulation each cryostat can operate more than 24 h without refilling LN_2. The different HTS Maglev train concepts in Germany, China and Brazil are compared in section 3.7 together with a proposed Maglev magnet configuration.

The objective of this paper is to review the status of bulk magnet interactions including vacuum and cryogenics to meet industrial-like parameters like volume, weight, speed, power and cost. For magnetic applications with HTS it is important to retain an engineering perspective in the future, to consider interdisciplinary project work and the inherent complexity including HTS properties, cryogenics, energy density, compact design, strain, stress and magnetic pressure.

We observe a clear eigendynamics in working with HTS innovations. The large-scale use of superconductivity continues to be dominated by applications for which there is generally a conventional technical option, while in some fields like fusion and high energy physics HEP superconductivity has enabled new science and technology that could not exist without it. Although superconductivity is an enabling technology for these fields, it comes with a number of challenges and targets, and direct market penetration has been very slow and is often not necessary. The situation with bulk superconductors is completely different. The magnetic fields required here are smaller, say 1–5 T instead of 10–20 T in HEP. The challenge in the fields of power energy and mechanical engineering is to compete and to accomplish the long-standing technical standards. In this field it is much more difficult to replace existing conventional technologies.

This paper summarizes the current status of large-scale applications of bulk superconductivity, using magnetic bearings, flywheels and transportation technology. We try to examine the key technologies, the prospects and challenges for new bulk HTS large-scale applications in the future.

2. HTS bulk materials

2.1. Melt-textured growth process

Bulk YBCO with large domain size and high intra-domain critical current density has been developed by different melt processes such as melt-textured growth (MTG), quench melt

Figure 1. Single-and multi-seeded melt-textured YBCO bulks.

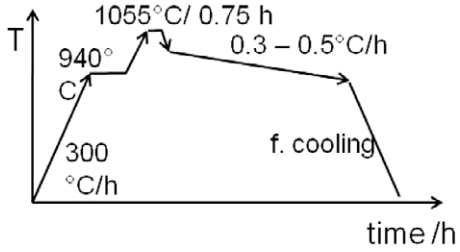

Figure 2. YBCO melt-texturing temperature profile in a gradient temperature furnace.

growth (QMG), melt powder melt growth (MPMG), powder melt growth (PMG) and oxygen-controlled melt growth (OCMG) including numerous variations of the processes. Among this fabrication single crystals or domains with dimensions up to ⌀50 mm × 15 mm are prepared routinely by top seeding methods. Bulks up to 100 mm size are possible by adapting a corresponding temperature profile. For successful large sample diameter growth the peritectic temperature T_p of the powder mixture has to decreases with the diameter of the large sample, e.g. by mixing different RE species. The samples are sensitive to mechanical forces and are typically selected from a furnace batch. Besides large crystals and magnetic domains the applicability is determined by microstructure engineering. The non-superconducting RE 211 phase, preferred in a nanoscale size, provides therefore a basic pinning background. A second type of pinning is associated with doping selected elements. This doping generates a spatial scatter of the superconducting transition temperature T_c throughout the sample. Zn-doped YBCO melt-textured bulks follow this mechanism whereby Zn atoms replace Cu sites. The result is an increase of the critical current density J_c at fields of 1–3 T. The J_c (B) curves show the typical peak effect in the J_c versus B measurements. It seems generally accepted that the same peak effect is obtained for solid solutions of binary or ternary compounds like (Nd, Eu, Gd)–Ba–Cu–O with composition variations in the matrix providing regions with weaker superconducting properties or causing disorder in the oxygen sublattice. Which pinning mechanism is most effective is still a matter of investigation.

Our HTS bulk material fabrication at the 400 kg pa level is performed by the top-seeding melt growth procedure (TSMG). Typical single-and multi-seed samples of ATZ fabrication are shown in figure 1. TSMG is a well-understand melt-texturing process studied and improved in the last decade in many HTS groups. A summarized report is given in a monograph in [29]. Light rare earth (LRE = Sm, Gd and Nd) materials with generic thin film seeds (Sm123, Nd123) and processing in reduced oxygen atmosphere are coming into focus [8, 30]. In particular, GdBCO bulk samples prepared by cold seeding seem to have high J_c values at 77 K. For tests we have started to fabricate 30 mm GdBCO bulks on a small-scale level recently.

ATZ's basic process is the melt-crystallization process carried out with precursor mixtures of Y123 + 32 wt% Y211 + 3–10 wt% Ag. All rare earth (RE) precursors are produced in-house with RE_2O_3 (RE = Y, Sm, Dy and Gd), $BaCO_3$ and CuO powders via multiple calcination steps. The addition of 0.6 wt% CeO_2 is effective in influencing the microstructure and to refine the Y211 particles. Because of increasing costs PtO_2 doping is reduced stepwise in our production. A highly efficient planetary mill (Type RETSCH PM 4000) with up to 300 rpm is used by us to fabricate ultra-fine-grained Y_2BaCuO_5 precursor powders. Part of the powder is at the desired nanoscale size level. The interaction of a magnetic vortex core with these extremely fine pinning sites gives a quasi-first 'basic or background' pinning level in the bulk. The mixed powders are formed into the desired shape by a cold isostatic compression method at 1.3 kbar. To achieve large-area melt-textured YBCO samples multi-seeding growth technology has been favored, selected and developed in the last few years. Because the superconducting and magnetic properties can strongly vary with the position on a sample the performance of the whole sample is important when applications are concerned. Micro-cracks, grain boundaries (GB) and weak links inside a bulk sample may cause a deterioration of the magnetic properties.

Table 1. YBCO bulk material parameters.

Parameter	value
Transition temperature T_c	92 K (−181 °C)
Specific resistance ρ_{300}	0.6–0.8 mΩ cm
Density (theoretical)	6.38 g cm^{-3}
Density (experimental)	5.95 g cm^{-2} (93%)
Specific heat capacity c_{300}	0.18 W s g^{-1} K^{-1}
ATZ calorimeter meas. c_{RT}	0.25 W s K^{-1} g^{-1}
Coefficient heat transfer λ	4 W m^{-1} K^{-1} ∥ c
	9 W m^{-1} K^{-1} ∥ a, b
	6–7 W m^{-1} K^{-1} poly
Lin. expansion coefficient	5–8 × 10^{-6} K^{-1}
Tensile strength	25–30 MPa
Critical current density J_c	10^4–10^5 A cm^{-2} (77 K, 0 T)

The typical growing procedure follows a temperature route after figure 2: heating up to about 940 °C for densification and pre-step reaction, further heating to 1055 °C (YBCO), 0.5–1 h dwell time, fast cooling to 998 °C and re-crystallization with a ramp-down of 0.3–0.5 K h^{-1} to 940 °C, cooling with 50 K h^{-1} or furnace cooling to room temperature. In the last step oxygen annealing at temperatures of 500–350 °C for 150–250 h is performed. Some estimated basic material parameters of our melt-textured YBCO are summarized in table 1.

Alternatively, the precursor powder for the melt texture procedure has a composition of $Y_{1.4-1.6}Ba_2Cu_3O_x$ following the Y_2O_3 excess route with a mixing procedure of 0.3 wt% Pt, 3–5 wt% Ag and 0.4–1 wt% CeO_2 [31].

2.2. Top-seeding technique

During the fabrication procedure geometrical effects can also influence the final performance. Sm123, thin film Nd123 or MgO (100) are generally used as seed materials, which have higher melting points than YBCO and comparable lattice constants. Sm123 seed crystals are prepared from SmBCO by the melt texture procedure. The seed crystals are placed on top of the surface (cold seeding) of the pressed YBCO samples followed by the heat-treated melt processing route. With the top-seeding technique high quality superconducting magnetic material in blocks of circular or rectangular shapes up to 60 mm can be fabricated in batches up to 30 large multi-seeded samples. If larger flat samples or samples with extended circular shapes are needed (rings, tubes and segments), they can hardly be grown in one crystal. One solution is to assemble them from well-shaped smaller bulks. After oxygenation the bulks are machined into the desired geometry, assembled, and glued in the corresponding frames and chambers.

Our standard three-seed YBCO bulk samples have a typical as-grown geometry of 67 mm × 34 mm × 15 mm. For precise assembling in magnetic applications the final size is milled with numerical machines and diamond cutting tools to $64 \times 32 \times 13$ mm^3 with a precision of 0.1 mm. Figure 3 shows schematically the three-seed bulk geometry and the position of the seeds. Due to the (a) and (b) misalignment in the geometry of the three-seed bulk (one would expect a sample length of 3×32 mm $= 96$ mm) we try to squeeze the crystal-growing front of neighboring crystals together to reduce the weak-link behavior of the two GBs. Thereby, in contrast to the top-seeding technique of a cylindrical sample, the exact lateral orientation of the square planar Sm123 seeds (3×3 mm^2) is an important parameter for the final superconducting properties of the GBs. The exact adjustment of the seed crystals orientation in parallel to each other on top of the green body determines the quality of the total multi-seed sample. The performance of the individual GBs in carrying inter-grain current depends on the epitaxial connection of the two neighboring crystals and domains. Larger samples with two rows of seeds, like the eight-seed samples in figure 1, have GBs in the [100] and [010] directions and are even more sensitive to the exact lateral position of the seeds on top of the green body.

Improvements in multi-seeding followed the question: which seed geometry is more sensitive to the current flowing through the corresponding grain boundary? The results are demonstrated in figure 3 from a qualitative observation of three-seed bulk crystal shapes. A top-seed orientation in the [100] direction indicates that the GBs are more homogeneous over the total joining surface without distortions between the crystals. A [110] seed orientation in contrast very often causes parasitic grains or growth distortion in the corners of the neighboring crystals as shown in figure 3. This observation is different to SmBCO thin film experiments on YBCO where

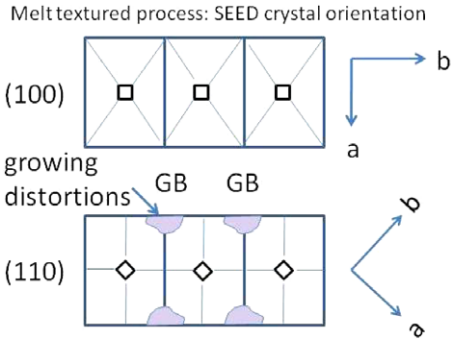

Figure 3. YBCO multi-seeding orientation (SmBCO seeds).

[110]/[1$\bar{1}$0] grain boundary formation was observed to be clean without a trapped liquid phase [32].

2.3. Bulk magnetic force

At the beginning of the bulk material characterization the magnetic force against a (standardized) PM was measured. The principal force exerted by a magnet on a superconductor is given by the gradient of the volume integral $F = -\mathrm{grad} \int (\boldsymbol{M} * \boldsymbol{B})\, \mathrm{d}V$, where $\boldsymbol{M}$ is the magnetic moment of the superconductor and $\boldsymbol{B}$ is the magnetic flux density produced by the PM configuration. The maximum levitation pressure is $P_{\max} = B_r^2/2\ \mu_0$, if the critical current density is infinity ($\mu \to 0$). However, levitation measurements are sensitive and depend on the flux density of the PMs used, on the magnetic distance variation and on displacement speeds. Therefore, the estimation of the trapped field distribution seems a more adequate and reliable parameter of the quality of the HTS bulk material. Results of a corresponding round-robin test with a 5% level spread give confidence for the reliability of trapped field measurements even between different laboratories [33]. Even if the situation is contradictory in so far as we utilize the HTS magnetic forces for most of the bulk applications the trapped magnetic flux is the key parameter of characterization of the material quality.

2.4. Trapped field distribution

A better bulk performance is given by increasing the critical current density J_c as well as by the length scale over which the currents flow. Both factors determine the field trapping ability which is improved in the last decade routinely to maximum values above 1 T at 77 K, passing the maximum field of high energy permanent magnets NdFeB and SmCo. Our trapped field measurements of YBCO samples of 46 mm diameter after relaxation shows values of $B_{\mathrm{trap}} = 1.2$ T at 77 K at 0.5 mm distance. The most important parameter is the critical current J_c, which is coming close to 10^5 A cm^{-2} in the self-field and several 10^4 A cm^{-2} at an external flux density of about 2 T. Since the superconducting current flows throughout a single domain material without distortions, large magnetic moments can be produced. Other RE123 materials with extremely fine-grained 211 phases, like Dy123 or Gd123, can trap up to 3 T at 77 K [4].

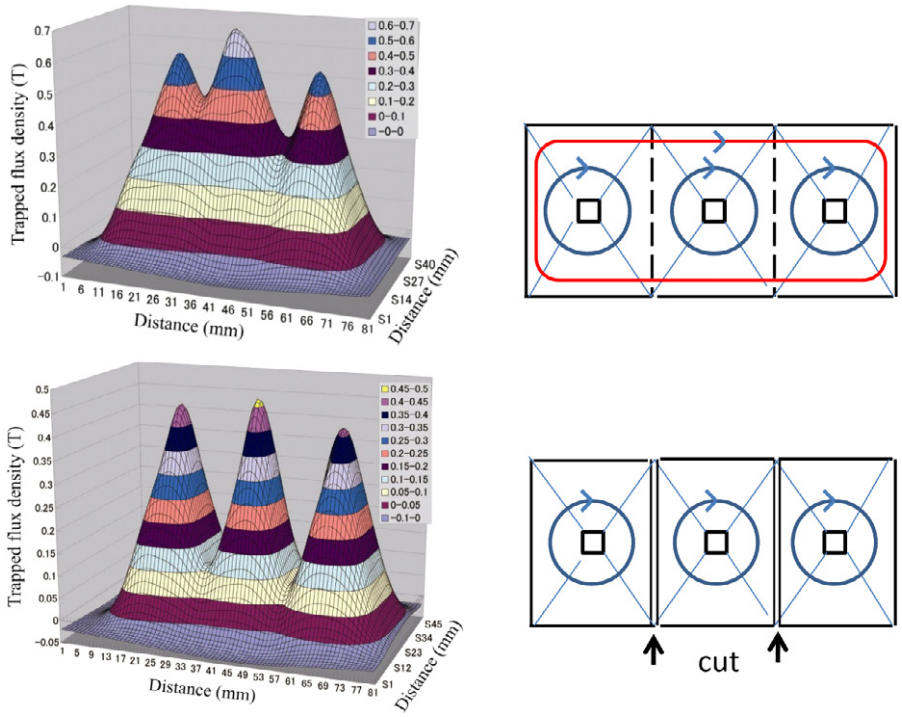

Figure 4. Trapped field measurement of three-seed YBCO bulk as-grown (top) and after cutting along GBs.

Although numerous RE123 compounds (RE = Y, Nd, Sm, Dy and Gd) in the basic composition $RE_1Ba_2Cu_3O_{7-\delta}$ were synthesized with excellent superconducting properties and T_c temperatures between 90 and 93 K for most applications $Y_1Ba_2Cu_3O_{7-\delta}$ (Y123) is the base material for large-scale magnetic applications. In addition, economic arguments cause low-cost and recycling attempts in the fabrication which is useful, especially in large-scale applications. Here tens of kilograms of valuable melt textured bulks are often necessary and used.

For bulk characterization the established and preferred measurement is the field-cooled (fc) method in the presence of an external magnetic field created by an electromagnetic coil or PM. Part of the external field will be trapped in the superconductor. After relaxation the material is characterized usually at 77 K by field mapping of the trapped magnetic field above the sample surface using a miniaturized Hall sensor. The step widths are 1 or 2 mm and for large samples the measurement takes one hour or more. Higher fields can be trapped by reducing the temperature of the bulk superconductor. For applied fields above 5 T, cooling down and heating up has to ramp at low rates to avoid thermally induced flux jumping. Such flux jumps can cause material cracks due to the high Lorentz forces.

Pulsed-field excitation is another technique to deposit a magnetic flux in the HTS. Using iteratively magnetizing pulsed-field operation with stepwise reduced amplitude (IMRA method) the maximum magnetic field of about 3 T at 30 K could be trapped [34].

A trapped field distribution with three peaks of a three-seed YBCO crystal at 77 K is presented in figure 4. The shape of the distribution indicates a threefold domain structure without significant macro-cracks. For the levitation pressure the averaged magnetization is more important than the peak values. To increase the material quality for large-area magnetic bearing purposes it is common to select single-domain bulk samples and assemble them into the desired shape and area. Alternatively, large-sized high-performance melt-textured bulks with multi-seeded domain structure increases the average trapped field value. Correspondingly, the quality of melt-textured YBCO components of magnetic stators was improved through processing larger blocks with multiple seeding on the surface. Due to this near-shape as-grown strategy, the assembling and machining effort for the final shape and function is reduced.

In recent bulk cutting experiments, the multi-seed results are apparently distinguishable from the bulk combination with isolated single-domain bulks. The measured trapped flux density in the connection areas between the crystals gives evidence that the GBs between the grains are strongly connected or coupled inside the multi-seeded bulk. This indicates that a finite supercurrent seems able to pass the GB, that is, the inter-grain current is considered in macroscopic dimensions (figure 4). The beneficial inter-grain current increases the total trapped flux by 40% [35]. Moreover, by systematic polishing experiments of multi-seeded samples from the seed surface stepwise 1 mm down a strong GB coupling was found to always exist along the *c*-axis growth. In a simple model we assume two kinds of supercurrent flowing inside the whole multi-seeded bulk, after figure 4 (right hand). After cutting along the GBs and assembling the three separate individual grains the trapped flux measurement

displays three well-separated peaks with substantially lower intensity. The coupling magnetic flux is now almost at a zero level, indicating the obvious and expected situation. This result is very promising for practical applications of the multi-seeded bulk.

In the next step, we will notice briefly another material performance often disregarded when discussed HTS applications. However, the working limitations in trapped field magnets or levitation devices are severe and have practical consequences.

2.5. Mechanical bulk properties

The magnetization and cooling-down process is extremely sensitive at large magnetic fields. High fields generate Lorentz forces which may cause distortion in the crystalline and domain structure. The maximum trapped field is not only limited by the magnetic properties of the material rather than by the produced internal magnetic stress and force. This force passes the tensile strength limit of the HTS material with about 30 MPa already at about 3 T. The stress is a Lorentz force between the trapped field B_0 and circulating current loop $\mathbf{A}_c = \mathbf{B}_0/\mu_0$ of magnitude $\sigma = \mathbf{A}_c \times \mathbf{B}$ (N cm^{-2}). Therefore, higher fields often cause material fracturing accompanied by drops in the magnetization curve. In order to prevent mechanical damage the samples are armed under pre-pressure by a steel or carbon fiber bandage. Further on, the tensile strength of bulk YBCO superconductors can be improved by vacuum epoxy resin impregnation and wrapping with a carbon fiber fabric [36, 37]. Due to the stabilizing technology the internal stress during magnetization, e.g. from 7 to 0 T at 65 K, is reduced from 150 to 40 MPa. In addition, resin impregnation enhances the mechanical strength of melt-textured YBCO by a factor of 2.5 and with 60–80 MPa at 77 K the material strength approaches the adequate properties required for most magnetic applications.

We have developed a copper deposition technique in general for HTS surface plating [38] and stabilize bulk materials by additional thermal diffusion of the copper into the bulk. Because Cu atoms are small the surface layer diffuses into small holes and cracks in the near-surface bulk and contributes to a better mechanical stability. The method can be used in combination with or without resin impregnation.

3. HTS magnetic bulk application

3.1. Magnetic bearings

High-T_c superconducting magnetic bearings (SMB) are larger than conventional steel bearings and show a higher complexity (magnet, superconductor, cooling, insulation and housing). The presently obtained force density is about 10 N cm^{-2} and much smaller than the 10^3–10^4 values of mechanical bearings. Active magnetic bearings (AMB) show force density values of 30–40 N cm^{-2}. However, simply having a high temperature superconductor and a permanent magnet does not produce a bearing that will support a motor or flywheel rotor. The design of the HTS magnetic bearing is of fundamental importance for achieving large electromagnetic forces and stiffnesses. In addition, it is difficult to conceive a rotor technology with constraints that include four or five degrees of freedom, while allowing it to rotate freely without friction about its principal axis.

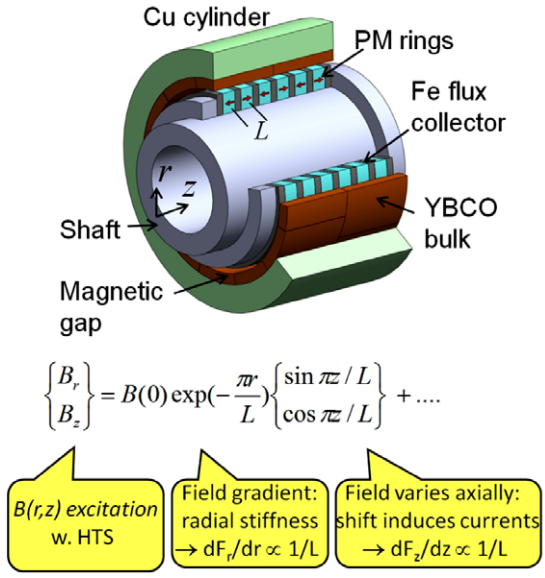

Figure 5. High-gradient magnetic bearing design.

Thrust bearings in the bottom and/or top positions interact axially with permanent magnets and have been frequently tested for man-loading demonstrators and flywheel purposes. Usually, the HTS magnet stator is composed of an array of small, single-grain YBCO tiles in a plane. This axial geometry is easy to manufacture and shows advantages in cryogenics. However, due to the lateral extension, it limits the compactness of the bearing, the force, stiffnesses and maximum rotor speed due to the acting large centrifugal forces.

The design and physics of HTS bearings have been reviewed and described in a number of papers [10–12, 16]. The bearing-interacting magnetic forces are usually studied by more or less idealized geometrical simplifications, such as the single-magnet interaction [39] or restrictions to plane-parallel arrangements [40]. The calculations reached several conclusions of how the force and stiffness of a bearing can be optimized.

3.2. High-gradient magnetic bearing design

Figure 5 shows the principal design and the rules for an optimized magnet excitation of a radial and axial high-gradient HTS bearing after our investigations. The magnetic distribution of the vectors $\mathbf{B}_r$ and $\mathbf{B}_z$ can be calculated by the expression of figure 5. After that, the field decays with the exponential function along the radius vector r and relative to the axial distance of the magnet poles L (pole pitch). This field gradient determines the radial force F_r and stiffness dF_r/dr. The sin / cos function covers the periodic field variation in the axial direction and determines the axial force and stiffness of the magnetic bearing.

In practice, rotor designs utilize the above-described magnet arrays rather than a single permanent magnet.

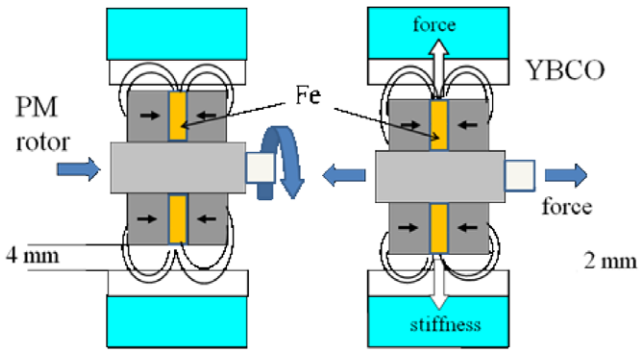

Figure 6. HTS bearing force generation by displacement of the magnetic rotor versus the superconducting stator.

Moreover, numerical FEM calculations are not so restricted and can be used for various geometries and current distribution models. It has been shown that subdivision of the magnets in a multi-pole arrangement with the pole pitch L in figure 5 can increase the stiffness provided the air gap can be kept small. From the calculations for small magnetic air gaps <2 mm the combination of PMs with soft iron collectors between them seems to be of little benefit [40]. The enhancement of the electromagnetic force due to Fe collectors vanishes at medium gap distances and reverses at smaller gaps <2 mm.

Many scientific and technological groups studied carefully and reported about force measurements by varying the PM configuration of bearings, such as the number of poles, the thickness of the PM and the shape of the HTS. They found no clear behavior of the force density on the PM configuration and conclude that the optimal magnet configuration is a strong function of the gap at which the system is operated. In addition, due to the finite size of both the PMs and the superconductors, edge and surface effects may influence the levitation force. For larger magnetic distances >4 mm the combination of permanent magnets (PM) with soft iron collectors between them is the ultimate. Thereby, the Fe shims or rings not only collect, amplify and homogenize the magnetic flux but turn the flux into the direction of the superconductor parallel to the crystallographic c axis. Due to the Fe collectors the maximum magnetic flux is limited to about 1.8 T because of saturation effects. Typically, larger gaps become necessary because in HTS magnetic bearings the forces and stiffnesses are generated by displacement. Figure 6 shows the effect of force generation by 2 mm radial displacement. If forces are specified one should reference them to a certain displacement in the axial or radial bearing directions. In an internal convention, we determine force and stiffness parameters typically at a rotor displacement of half of the free-space gap, typically 2–3 mm.

While the principal magnetic interaction is well understand, the practical design of the bearings is still a task and work of high complexity and challenge. Because the magnetic bearings must operate unattended continuously and reliably under high mechanical moments and forces, thermal insulation and high mechanical stability is required. An important feature of all HTS bearings is the cryogenics either with LN_2 or cryocooler machine cooling. Fabrication technology with integrated cooling requires the construction and engineering

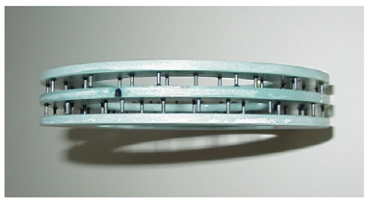

Figure 7. Constructed glass fiber platform; diameter 150 mm, max. load 20 kN, thermal loss (RT to LN_2) $Q \sim 0.3$ W.

of a low weight, nonmagnetic stainless steel or G-10 bearing housing or cryostat. Ultra-low heat transfer structural elements were designed, measured and constructed for bearing stability up to forces of several tons. Figure 7 is a photograph of a 150 mm diameter G-10 platform with 2 × 42 pins@6 mm lengths to support a cold superconductor stator ring under high axial loads. The maximum axial force is 20 000 N at a low thermal heat transfer from room temperature to LN_2 of <0.3 W. The axial stiffness of these glass fiber platforms is estimated to be about $k = 175$ kN mm^{-1}.

Another direction of development of HTS bearings is technical up-scaling for increasing weights and loads. An advanced radial PM rotor excitation design together with a 5 kg melt-textured 200 mm sized assembled YBCO ring were fabricated by ATZ for application in a German flywheel project. The magnetic field of a rotating device is basically generated by permanent magnets (PM), which are attached to a shaft. Alternatively, Cu or superconducting solenoids are used for magnetic field generation. Clearly, for rotating systems the coils and solenoids need electric power, transfer connectors and mechanical stability against dynamic forces when in rotating operation. Therefore, at least in rotating bearings the use of permanent magnets is easier to realize and presently preferred instead of energized coils.

For heavy-load applications we produced a number of 200 mm HTS bearings. Permanent magnet rings (NdFeB) in the geometry ⌀200 mm × ⌀150 mm × 8 mm, are axially stapled to the inner rotor shaft. Their individual magnetization is in the axial direction, whereby the value of magnetization varies, about a 360°-circumference turn, by ∼4% of the maximum value. The PM rings are assembled in opposite polarity (on pressure) causing a radial flux distribution of a high magnetic flux gradient with the adjacent superconductor. The PM configuration of the magnetic bearing is explained in figure 5. One important parameter is the temperature of the superconductor. The magnetic forces are increased with lower temperatures and the force–displacement curve bending observed for 77–80 K disappears due to better pinning performance. While in figure 8 the 79 K force–displacement curves are more or less flattened at larger displacement (part of the pinned magnetic flux is stripped off from weaker pinning centers), at an optimal magnet configuration the 72 K curves are almost linear with displacement. The PM–Fe geometry for the given air gap of 3 mm is optimized by variation of the PM/Fe thickness.

At the best PM 12/Fe 6 configuration magnetic forces over 10 000 N axially and 4700 N radially were measured

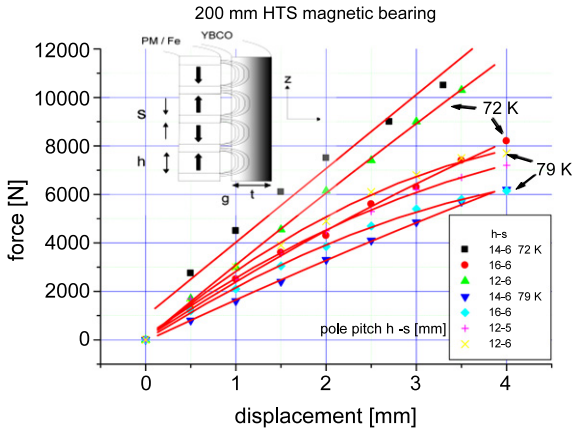

Figure 8. Measurements of axial magnetic forces with varying PM (h)–Fe (s) geometry at 79 and 72 K.

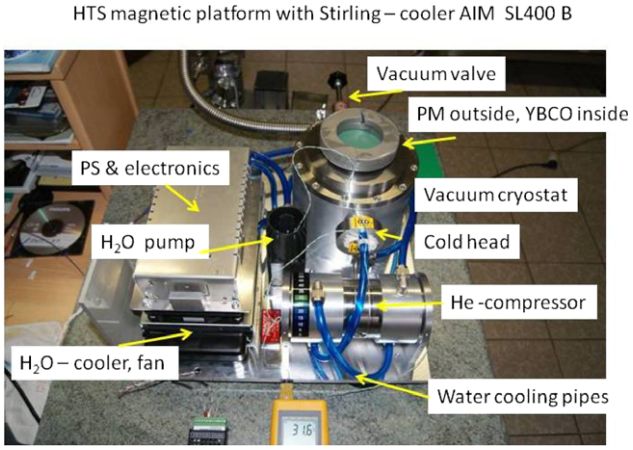

Figure 9. HTS magnetic platform with Stirling cooler AIM SL 400 B designed and constructed for mobile applications.

at an HTS temperature of 72 K (sub-cooled LN_2). With stiffness values of 4 kN mm^{-1} and 1.8 kN mm^{-1} in axial and radial directions, respectively, SMB technology approaches industrial requirements for heavier machinery like high speed motors, turbines or flywheels.

What is the future SMB development? Physically it is clear that the magnetic excitation due to PMs is basically limited by the available coercive force of the PM material. This limitation is attempted to overcome by the use of LTS/HTS coils for excitation in magnetic bearings. Several groups in advanced laboratories are concentrating on HTS coil interaction with increased flux excitation [41]. The first success is reported by RTRI in Tokyo, e.g. for a 10 kWh railway flywheel [42]. A promising load capacity of 20 kN has been demonstrated at cusp fields of 5 T (NbTi coil) and 2.8 T (Bi2223 coil) against 60 mm GdBCO bulks, respectively. The disadvantage of the coil excitation is the necessity of low temperatures of 4 K and about 15 K, here provided by cryocooling.

3.3. Cooling

Finally, for safe SMB operation the integration of efficient cooling systems by cryocooler operation is necessary. In the developed flywheel ATZ–MM project (see section 3.4) the HTS top bearing was cooled by a 30 W Gifford McMahon (GM) cryocooler (type CP350 CTI Corp.) capable of cooling down the YBCO stator to 50 K. The lower temperature improves both the load performance as well as the long-period stability of the superconducting bearing. On this flywheel we report more details in section 3.5.

A recent mobile demonstrator platform in figure 9 with four melt-textured YBCO bulks (mass 650 g) was attached with an AIM SL 400 Stirling cooler with nominal performance of 4 W cooling power at 80 K. We are investigating two questions: can we transform the magnetic bearing technology into mobile application systems? Is a compact and low-weight Stirling cooler capable of serving as reliable cryogenics for the bulk superconductors in this size? The He compressor part itself is cooled by a closed-cycled water circulation system developed separately by ATZ. The HTS bulks are assembled on an Al alloy desk thermally insulated from the housing ground by a mechanical support of glass fiber G-10 material. Surrounding vacuum and radiation super-insulation foils provide the necessary thermal insulation. The cold mass of 850 g in total consisting of YBCO and Al after 5 h Stirling cooler operation could be cooled down to a temperature between 40 and 50 K. The first experiences still showed some outgassing effects in the cryostat, lowering the insulation vacuum. After a short re-evacuation the platform with a levitated 100 mm magnetic ring operates safely at 50 K. The total thermal loss at a vacuum of 10^{-2} Pa was estimated to be only 1.2 W.

3.4. Damping

Finally, after considering forces, stiffnesses and cooling we like to mention an important and key property of HTS magnetic bearings. Because of the limited stiffness compared to mechanical bearings damping of unbalanced rotors is essential. Especially damping the oscillations at critical rpm's determine the applicability basically [14, 43, 44]. Principally, a rotating shaft in an SMB shows rotor oscillations which can be critical. If the air gap is small, say 1 mm or less, the free rotating shaft can have oscillations and amplitudes larger than the free gap and touches the surrounding HTS stator. Especially critical are the amplitudes of the eigenfrequency of a rotor [45]. The angular stiffness must be sufficient to limit any misalignment during operation. Another feature during operation of an HTS bearing is resonance or critical speeds caused by residual rotor imbalances. The bearing must limit the resonance amplitudes to prevent touchdown of the stator. In a catastrophic case, at high speeds large resonances or shaft bending modes can destroy a complete machine.

If one speeds up and accelerates a rotor at a certain speed fast increasing amplitudes are observed. This is usually the eigenfrequency situation observed in all rotating machines in mechanical engineering fields. The rotor passes a phase jump from sub-critical to over-critical rotation movement. Above

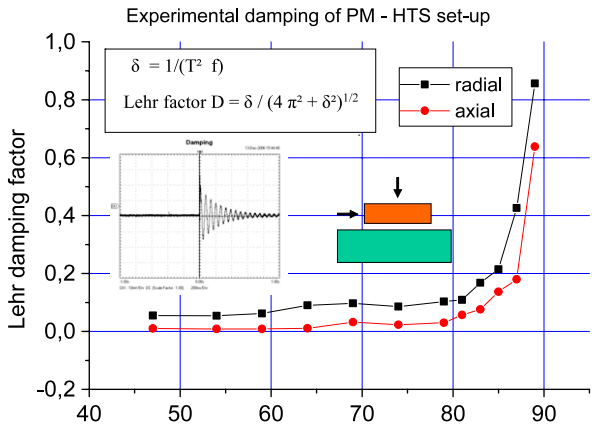

Figure 10. Experimental vibration and damping results of a 100 mm PM ring above the YBCO block cooled by a Stirling cryocooler.

the phase jump frequency ω_c the rotor is always rotating self-centered on the center of gravity with the additional benefit of a 'balancing effect'. Under circumstances, a fast operating rotor must be spaced sufficiently from the resonances. A speed factor of $\sqrt{2}$ from the critical frequency ω_c is well experienced for save operation.

For vibration testing and damping performance estimation we investigated different magnet–HTS configurations. We used an axial bearing like in figure 9 with a 100 mm PM ring on top of the cryostat. The levitated PM ring was excited by a hammer impact and an accelerometer measures the frequency range of interest and their size as the rotor response. The mass of the accelerometer has to be small compared to the rotor size and weight.

Measurements of the damped oscillation are plotted in the inset of figure 10 and converted into the frequency domain which is the discrete Fourier transform of the time domain signal. A measure of actual damping can be obtained from the logarithmic decrement. The (Lehr) damping factor D is a function of the temperature of the bulk HTS. It is less than 5% for LN_2 temperatures or lower. We found a steep increase of the damping above 85 K where the hysteretic loss is the main damping contribution. The damping performance curve with temperature follows the inverse J_c value of the HTS material. The measurements demonstrate the common experience with SMBs. The damping performance at the typical temperatures of magnetic bearings (LN_2 or lower) is too low for a safe operation of high energy rotors. Unfortunately, the high damping properties cannot be utilized because at these temperatures J_c and hence magnetic forces and stiffnesses are far from any application.

For solving the problems we have been developed passive damping systems combined with magnetic rotors.

Superconducting magnetic bearing tendencies:

- Journal bearing-type high-gradient magnet design.
- Integrated and 'invisible' cryogenics, integrated damper.
- Attached mechanical emergency bearings for warm support, rotor confinement, safe operation.
- Higher magnetic flux density excitation (coils).

3.5. Flywheel energy storage system (FESS)

Flywheel energy storage systems (FESS) are suited for the storage of electricity and have already been applied for a number of years using mechanical bearings. In 1988 flywheels of 2 kWh/150 kW from Magnet-Motor Corp., Starnberg, Germany were first applied in two communal diesel-electric buses in Munich, Germany. Further diesel-electric demonstration buses followed. In those years experience could be gained on the operation of flywheels in vehicles, their interaction with the electric propulsion system, the potential of energy saving in buses, reliability and maintenance needs. One important result was that energy savings of 30–35% can be obtained if you regard only the energy balance of the diesel-electric propulsion system including the flywheel. In 1994/95 a small fleet of 12 trolleybuses in the Swiss city of Basel was built, equipped with flywheel units to relieve the overhead network and to recover the brake energy on-board. These buses have been in operation for more than 12 yr. Most of these flywheels have operational hours of more than 50 000. They operate very reliably, provide energy savings of 20–25% and have an MTBF of about 38 000 h, which means that a repair on a flywheel is necessary only every 8 yr. Today, small-scale FESS with storage capacities less than 1 kWh are produced by Vycon Corp., Pentadyne and Active Power (all USA). The steel or composite rotors are stabilized here by active magnetic bearing systems (AMB).

With the progress and the availability of superconducting passive magnetic bearings some larger FESS projects have been performed in the last few years: a 5 kWh/100 kW Boeing flywheel energy storage system [45], the NEDO 10 kWh/100 kW flywheel project [46], and the 5 kWh/250 kW ATZ-magnet-motor (MM) flywheel system [47]. While the first project (Boeing) uses the suspension of an axial HTS magnet bearing at the bottom, the two other FESS are equipped with strong journal HTS bearings of 200 and 175 mm diameter to stabilize the rotors. The NEDO flywheel possesses in addition an upper and a lower radial AMB (Koyo Seiko) to stabilize the 380 kg rotor.

In stationary applications purely magnetically stabilized flywheels offer a number of advantages. Maintenance at the flywheel is only necessary once in a longer time, losses are minimized and non-contact, very low noise operation is possible. In the field of magnetic bearings the high temperature superconducting (HTS) bearing is definitely the most fascinating and promising technology. Due to its physical properties it needs no electronic controller and operates completely passively. The SMB is inherently fail-safe in contrast to AMB after power loss. Using liquid nitrogen as a cooling fluid the HTS superconductor is operated at fairly low temperatures, far below critical operation points, and is therefore safe and reliable. In the usually performed comparisons between two superconducting devices, SMES and HTS flywheel, our calculations and evaluations show the flywheel as a better and more robust solution for the future electricity storage situation, even for pulsed power applications.

Especially valuable is a FESS coupling with solar tiles and windmill generators. It contributes to achieving maximum

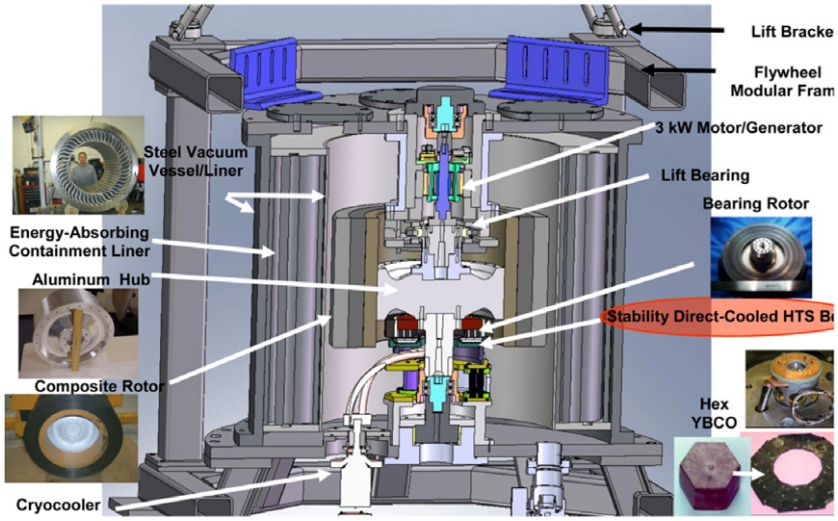

Figure 11. Design of the Boeing flywheel energy storage system with critical components [45].

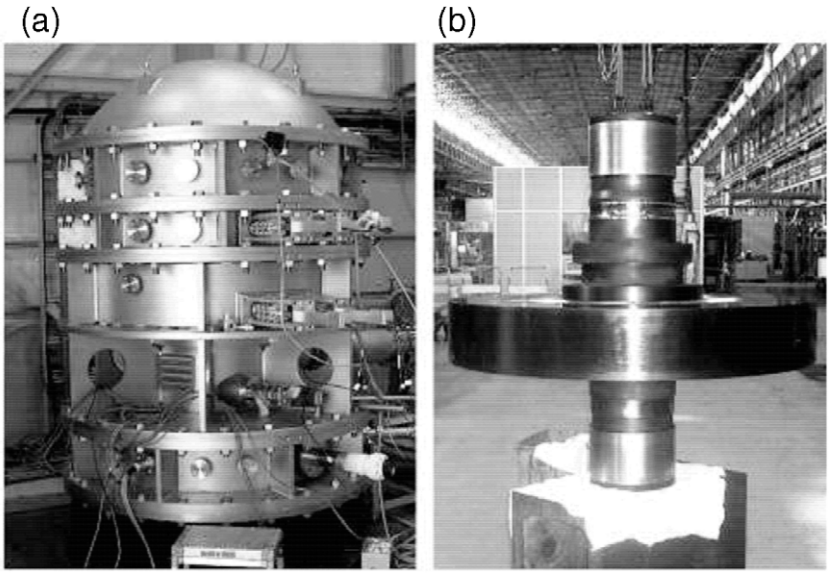

Figure 12. NEDO test flywheel energy storage system with composite rotor [46].

energy capacity and energy yields. The combination prevents DC over-voltage, frequency and voltage regulation and contributes to grid stability. For successful UPS application the time to full power should be electronically switchable in 2–3 ms in order to stabilize frequency and voltage in the case of power failure.

Figure 11 displays the design of the Boeing 5 kWh/3 kW flywheel with important technical components and features [45]. The magnetic bearing consists of melt-textured YBCO bulks assembled in a ring shape. The 164 kg flywheel rotor is suspended totally passively by a permanent magnet (PM) lift bearing and the lower axial HTS bearing. The stator consists of YBCO bulks in the hexagonal geometry with a tip-to-tip dimension of 36 mm glued into a Cu holder and conduction-cooled by a cryocooler. The radial bearing stiffness from the resonant frequency is $k_{\mathrm{radial}} = 131\ \mathrm{N\,mm^{-1}}$. This relatively low stiffness value can be explained by the small number of pole pitches (three iron collectors) of the magnet excitation system. Boeing uses a PM clutch bearing with a near-zero stiffness to suspend the rotor weight. The PM lift bearing is located near the top of the rotor and has to be adjusted carefully to prevent a large negative stiffness on the HTS bearing.

The Japanese NEDO flywheel storage system was tested up to a speed of 11 000 rpm (5 kWh). Except for the HTS radial-type magnetic bearing near the 125 kg composite flywheel body two active magnetic bearings (AMB, Koyo Seiko) in the upper and lower positions stabilize the rotor and keep the resonance amplitudes small (<1 mm). In addition, a PM clutch in the attractive configuration reduces the weight of the rotor but causes a negative axial stiffness. The test flywheel is shown in figure 12 together with the composite rotor. It is interesting to note that the HTS bearing shows a force density of 10 N $\mathrm{cm^{-2}}$@77 K and 17 N $\mathrm{cm^{-2}}$@62 K at a magnetic gap

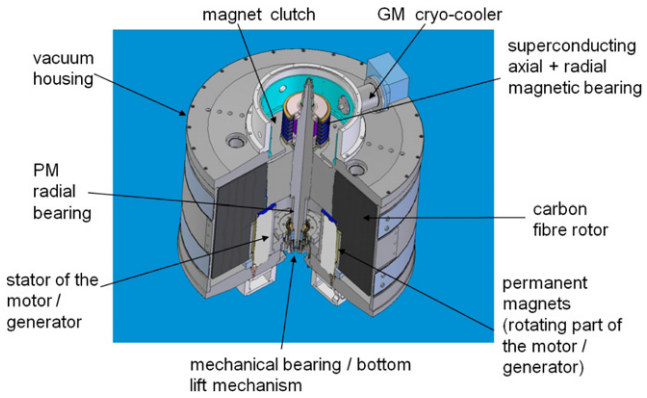

Figure 13. Outline sketch of the 5 kWh/250 kW ATZ–L-3-MM HTS flywheel.

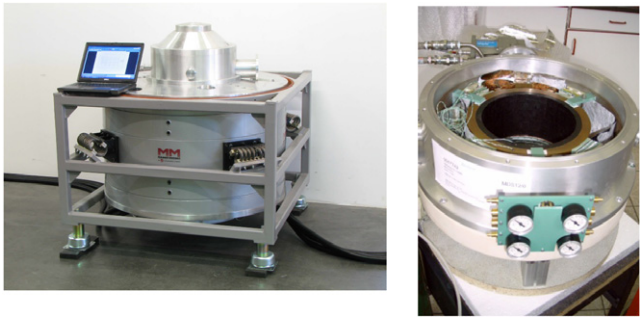

Figure 14. Assembled ATZ–MM compact FESS in frame with the top HTS magnetic bearing (right).

Table 2. R&D development costs of HTS flywheels.

Institution/project	(million US $)
Boeing, USA	∼20
NEDO consort. JP	∼35
Nexans & Piller, GER	∼10
Kepri project, KR	∼14
ATZ/MM, GER	∼2.3
NEDO, LTS, JP	∼25

of 0.8 mm. The rotational loss was 68 W@6000 rpm and 77 K, mostly caused by the AMB function.

ATZ and L-3 Magnet-Motor (MM) have developed a 5 kWh/250 kW flywheel energy storage system based on the conventional magnetodynamic storage (MDS) unit of MM. The flywheel system is extremely compact in design and construction and has a vertical rotation axis. The rotor is a hollow cylinder and is made primarily of a carbon fiber compound. To make the system compact, the motor/generator (M/G) unit is integrated concentrically in the cylindrical rotor. Figure 13 shows a section of the design principle of the HTS flywheel.

The system stores energy when the motor/generator M/G unit works as a motor and increases the speed of the rotor. The system delivers electrical energy when the M/G unit is switched to generator mode, thus reducing the rotor speed.

An energy capacity of 10 kWh is obtained at a speed of 10 000 rpm. In rotor test runs and calculations the critical amplitudes were larger than the limit of 0.5 mm. The original carbon fiber rotor displayed vibrations in the millimeter range in a test chamber. Redesigning increased the weight of the composite rotor including the motor magnets to 600 kg and hence substantially heavier than the rotors in the Boeing and NEDO flywheels. Although we could shift the critical rigid body frequency of the rotor to lower values below 1000 rpm still the vibration amplitudes were considered too large (0.8–1.4 mm). With the 20 year's of flywheel experience of the MM team it was decided to damp and confine the critical amplitudes by a dynamical operation of the mechanical emergency bearings at both ends of the rotor [43].

The integrated permanent magnet-motor/generator unit operates with a maximum power of 250 kW as a motor as well as a generator. The diameter of the evacuated flywheel housing is 1 m and the height is also 1 m. The weight of the complete flywheel unit is about 1200 kg plus the external periphery such as power electronics and cooling system. Figure 13 shows an outline sketch of the concentrical flywheel body without the vacuum housing.

The SMB developed and manufactured by ATZ is located at the top of the flywheel (figure 14). It consists of stacked high temperature superconducting YBCO three-seed bulks forming a hollow cylinder and glued into a copper tube. The YBCO is cooled by a 30 W GM cryocooler via conduction-cooling the copper. Inside the superconducting cylinder, rotating permanent magnet rings of size 200 mm × 150 mm × 8 mm are arranged and stacked around the shaft according to the design rules of figures 5 and 8. The PM rings and Fe collectors are concentrical to the superconductor ring. The magnetic forces could levitate completely the weight of the rotor (about 600 kg). The 200 mm HTS bearing with 1.8 kN mm^{-1} radially and 4 kN mm^{-1} axially provides the necessary stiffness too. Like in the previous flywheels of Boeing and NEDO the rotor is suspended and attracted by a magnetic clutch (PM–Fe) below the HTS bearing.

Because of the worldwide energy discussion and the obviously great challenge to store electricity in large amounts, being efficient, safe and reliable with constant capacity the flywheel efforts can contribute to solutions. However, the development costs are not small. We have estimated the costs of the above three flywheel projects with HTS bearings together with some further joint FESS projects and summarized them in table 2.

3.6. Flywheel electrics

The rotor's mass moment of inertia and its maximum permissible rotation speed determine the energy capacity of the FESS. The power capability is determined by the specifications of the M/G unit and the electronic converter system controlling the M/G unit. The M/G unit is a permanent magnet excited machine operated with compact high-performance IGBT inverters and is especially developed for the application in flywheels. The machine was optimized for both low no-load losses and a very high efficiency of 92–95% (in motor operation as well as in generator operation) including the losses

of the inverters. As a result the round trip efficiency of the flywheel system is about 85–90%. The power consumption of auxiliaries such as the vacuum pump is not included in this calculation. A very important feature for most applications is the extremely high cycling capability. The expected cycle lifetime is in the range of 10^6–10^7 cycles.

The M/G unit has only electrical connections. No rotating parts have to be directed outside the unit; no gearing is necessary. By integrating this unit in a vacuum housing, the losses due to air friction are very low. The vacuum of 10^{-2} Pa is maintained by evacuating using vacuum pumps. This completely sealed operation of the active part of the storage unit guarantees a low noise level of the system. Another advantage of the sealed housing is the ability to keep any damages inside, caused by a failure of the flywheel.

Losses through friction are minimized by the magnetic bearings and the low vacuum. The estimated losses are less than 900 W at full idle. The power consumption of auxiliaries such as the vacuum pump is not included. The cooling of the stator of the M/G unit and of the inverters is a closed-loop liquid circuit, which means that no dirt can penetrate into the system. A standard liquid/air heat exchanger or liquid/water heat exchanger transmits the losses to the surrounding air. For operation it is advisable to run the flywheel in a cycle operation mode between 100% and 50% of the nominal speed (10 000–5000 rpm), independently of the technical possibility. In an UPS operation mode the FESS may run down to 25% of the speed. As the energy of the flywheel depends quadratically on the speed, the energy used in a UPS operation mode is as high as 15/16 of the stored energy.

The power coupling between flywheel and DC link is realized by special power electronic units. These electronics consist of three single four-quadrant IGBT inverters which operate the 12 phases of the MDS. The switching frequency of the inverters depends on various parameters and is up to 20 kHz.

Current and voltage measurements as well as a diagnostic routine are integrated in the power electronics. The power management evaluates the signals from the temperature (stator, bearings and housing), vibrations (of the rotor) and vacuum sensors. Additional important operational parameters from the power electronic are supervised. In case of a malfunction automatic reactions to the protection of the systems are initiated (e.g. the shut-down of the flywheel system, if predefined limits are exceeded). Every malfunction is written in a protocol list.

The power management is able to control the FESS according to its actual operational strategy. Control variables are external data, FESS operational data and directives of the user. Basic software for the flywheel operation is part of the system. The operational strategy is adapted to the user's requirements in the basic software. The further optimization of the operational strategy may be an option. It is possible to transmit signals like power or voltage directives over an analogous interface to the control station. Also digital signals, e.g. to select one of the operational strategies, can be send.

Flywheel energy storage with superconducting magnetic bearings tendencies.

- The present size 5–10 kWh is not optimal (25–50 kWh per unit is more effective).
- Modular fabrication and modular application is the future tendency and choice.
- Magnetic bearings preferred, no degradation with time, low maintenance.
- HTS and PM bearing/clutch, presently show increased fabrication costs (reason: RE powder costs on the world market increased by a factor of four in 2009–11).
- Price increase of carbon and glass fiber (airplanes, military application, wind turbines).
- G/M and electronic parts costs seem to be leveling off.

3.7. Maglev transportation

3.7.1. Maglev status. High-T_c superconducting magnetically levitated (Maglev) vehicles for future transportation possess substantial advantages like non-contact and low noise movement above a magnetic rail. In addition, the system shows no wear, no degradation at high speed operation, low energy consumption and environmentally friendly transportation. It should be noticed that Maglev levitation is not confined strictly to trains because airport and rocket launching runways may also be contemplated. A Maglev launch system would use magnetic levitation and acceleration of a vehicle along a track at speeds up to 1000 km h^{-1}. The vehicle would shift to rocket engines for the launch to orbit. Maglev systems could dramatically reduce the cost of getting to space because they are powered by electricity, an energy source that is available on the ground in contrast to rocket fuel that adds weight and cost to a launch vehicle. In parallel, we observe physical studies and programs starting to integrate high-T_c superconductors in electromagnetic launch and rail gun devices. Thereby, the main target seems the availability of systems with a high energy density and power which is the basic limitation for new high speed devices.

Maglev trains are famous, primarily due to their highly innovative levitation and transportation technology. Thereby, Germany and Japan were at the forefront of Maglev train technology and both were testing prototypes of their Maglev trains in the last 20 yr. Unfortunately, the German transrapid technique was given up, based on political and economical considerations. The transrapid technique with an electromagnetic suspension system is today commercially operating in the Shanghai Maglev train connecting the center with the airport.

The large Japanese version of a Maglev train uses an electrodynamics suspension system, which is based on repelling forces. The superconducting version has at present NbTi magnets. The LTS coil cryogenics is bivalent; on the one hand the low temperature allows a persistent current mode (like an MRT magnet) and saves energy. Disadvantage of the NbTi coils is the small temperature difference between the liquid helium temperature (4.2 K) and the critical superconducting temperature of the NbTi material (9.2 K). Hence, Japanese Maglev engineers expect technical and economic improvements with high-T_c superconductors.

Bulk superconducting Maglev trains in demonstrator versions have been designed and fabricated in the last 5 yr.

With the individual magnet design the forces are generated by the fc process at an axial distance of 30–20 mm with load decreasing the gap to 10–5 mm above the PM guideway. Although the total loads were approaching levels up to 8000 N [19, 20] the force density values with 2 N cm^{-2} are still limited. In addition, axial stabilization possesses generally low stiffnesses and hence low guidance forces perpendicular to the rail direction, too. To overcome these problems, improvements are desired to three parameter features: (i) a better magnetic guideway design, (ii) high quality high-T_c material (higher J_c and better pinning) and (iii) nearly invisible cooling of the Maglev by means of cryostats with long operational time.

Finally, it should be mentioned that an advanced Maglev train test drive facility, called SupraTrans II, has been successfully started in February 2011 in Dresden, Germany. The guideway consists of a total of 4.8 t PM material and is an 80 m long double-track oval circuit. A contactless linear motor unit between the tracks drives the vehicle with a maximum speed of 20 km h^{-1}. The total load of about 6000 N@10 mm distance is levitated by four cryostats with LN_2 cooling, each containing 24 blocks of multi-seed YBCO bulks [49]. The vehicle can levitate and transport two persons around the PM guideway.

In general, the magnetic rail has to provide a large magnetic force at a large distance. Along the guideway the field distribution has to be homogeneous to provide a low running loss. For optimizing the magnetic guideway different FEM calculations are carried out considering a minimum of PM material (cost) at a maximum of magnetic excitation field. In most cases, the levitation force is evaluated in the mirror method by assuming the superconductor to be perfect diamagnetic. While the rail design has been investigated in numerous papers [23–28], the construction of the superconductor part of a Maglev systems is investigated and reported rarely.

3.7.2. Magnetic guideway design. Let us first briefly mention the rail configuration status. Typically, the magnetic rail geometry is calculated in finite element models (FEM) considering the PM and Fe properties and assuming a perfect diamagnetic superconductor. Although the PM rail can be assembled with one or two rows of magnets with upward magnetization, better rail performance is obtained by collecting the magnetic flux using soft iron. The target is clear; technically generate high magnetic flux density and high flux gradients in the direction of the superconductor at an economical level. A standard rail configuration can be roughly approached by the geometry of figure 15. Our proposed geometry parameters and dimensions of the PMs and the iron collectors follow an FEM calculation and the practical experience in magnetic rail design. Correctly, an optimal PM/Fe design is a function of the actual gap width g. The PMs should have a small rectangular geometry ratio widths × height as 4–5 × 7. Let us assume a gap of $g = 8$ mm then the PM geometry should consist of a cross section 36 mm width × 56 mm height, while the PM length is arbitrary, say 50 mm. According to figure 15 the Fe collector should be 12 mm thick. Strictly, for a given

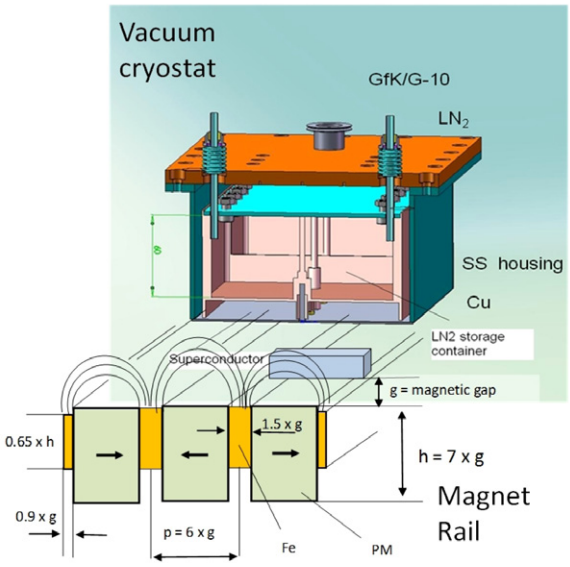

Figure 15. Maglev configuration consisting of magnetic rail and the HTS cryostat.

magnetic gap with the distance g between the surfaces of the PM and the superconductor only one corresponding magnetic geometry is the optimum design. Practically, the gap distance for the Maglev operation is assumed at $g \sim 8$–10 mm. It is recommended to calculate and design the rail geometry for a larger gap distance as the final expected levitation height, e.g. 15 mm. Our bearing analysis and studies show the necessity of 'pre-loading' for better forces, stiffnesses and stability.

In a next step improvements and advantages are obtained by the so-called magnetic Halbach configuration [48]. Here the Fe collectors are totally (full Halbach) or partial replaced by PM (partial or semi Halbach) with a magnetic polarization in the direction of the magnetic flux flow. This magnetic configuration generates a sinusoidal magnetic flux distribution over the rail cross section. Another peculiarity is a stronger flux distribution on one side of the rail compared to the other. In figure 16 a corresponding rail design is proposed and constructed by the HTS group of Jiaotong University [24]. Mechanically the array of PMs is difficult to assemble and to fasten but it is supposed to generate higher magnetic forces. For further magnetic rail improvements especially under practical and economical considerations it seems beneficially to combine the standard PM/iron configuration with the superior properties of the Halbach arrays in a hybrid rail type.

Clearly, the magnetic guideway is the most expensive part of a Maglev train. Independent of the different concepts for magnetic rail construction we calculated a cost factor of about 1.75 million US $ km^{-1} double track. Mechanical construction of the rails requires an additional 0.6 million $ km^{-1}.

3.7.3. Superconductor cryostats and vehicles. A number of experiments have demonstrated the feasibility of Maglev technology using superconducting bulks and PM tracks. Most experiments are performed by cooling the bulks located in

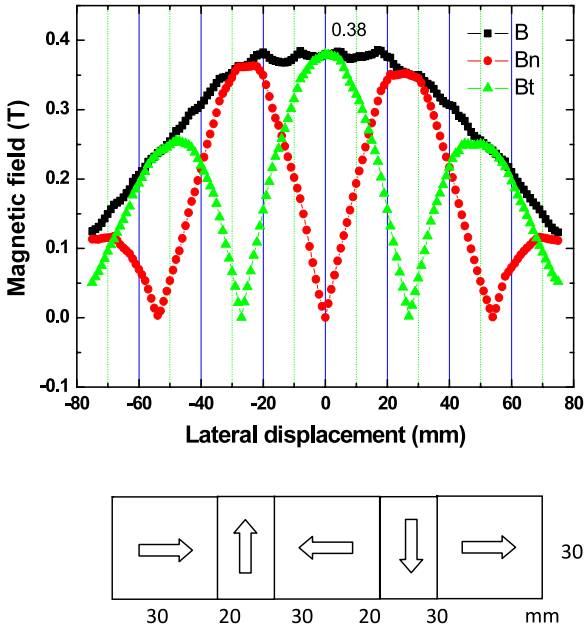

Figure 16. Halbach configuration and flux density distribution of the vector components calculated for 15 mm distance [24].

open vessels or containers thermally separated by Styrofoam. Because of the worse thermal insulation the HTS containers are cooled down in time and become covered with frozen layers of moisture. The corresponding loss of cooling power enhances the necessary cooling effort, usually by refilling LN_2 into the HTS container periodically.

An alternative solution for Maglev application is the use of vacuum cryostats reducing the cooling effort and increasing the overall efficiency. ATZ has developed a type of compact and mobile vacuum cryostat for a full-scale Maglev module. Usually four cryostats are mounted under a vehicle, achieving a magnetic load performance of 1 ton against a standard PM rail.

Up to now more than 30 vacuum cryostats shown in figure 17 were fabricated. The corresponding displacement versus force curves for different field-cooled positions are shown on the right-hand side of figure 17. Each cryostat consists of a stainless steel (ss) body with a G-10 plate on the top. A mechanical interface on top is provided to fasten the passenger module. The cryostats under the module vehicle are moveable in lateral directions/curves. Inside each cryostat 24 pieces of three-seeded YBCO bulks of dimensions 64 mm × 32 mm × 12 mm are glued and mechanically fastened in a copper holder. The total HTS area is about 490 cm^2 per cryostat. The superconductors are cooled using LN_2 stored in a chamber of the cryostat on the other side of the Cu frame (figure 15) by conduction cooling.

The 2 mm distance between the YBCO surface and the outer cryostat bottom is a technical highlighted feature and allows large levitation forces with respect to a high load capacity. Due to the 2.5 l LN_2 storage capacity long superconducting operation is ensured. Our measurements of the LN_2 consumption under static conditions indicate a one-day operation without refilling liquid nitrogen. Thermal loss measurements give values of Q_{loss} = 2.5–3 W per cryostat. Simultaneously, a compact and robust cryostat design and construction could be obtained.

Maglev train tendencies

- Material and cost-efficient magnetic guideway design.
- Module-like fabrication of magnet rail and superconductor device.
- Closed-cycle integrated HTS cooling (invisible).
- Semi- or Halbach magnet track construction.
- Maglev monitoring (gap, HTS temperature, speed, load).

4. Conclusions

Adelwitz Technologiezentrum GmbH (ATZ) has developed and built up, within the last decade, high-T_c bulk material fabrication to a level of more than 600 kg pa. All material fabrication like single-and multi-grain melt-texturing processes are application-oriented. Parallel large-scale applications have been studied and conducted in the fields of SMB technology. With the concept of high-gradient bearings using PMs the load capacity was verified up to 10 kN axially and 4.7 kN radially. Bearing variations and improvements include mobile systems, efficient cryogenics and low thermal loss vacuum cryostats.

A 5 kWh/250 kW flywheel energy storage system with a 600 kg composite rotor was constructed and tested. The tests confirmed the calculations and expectations of additional

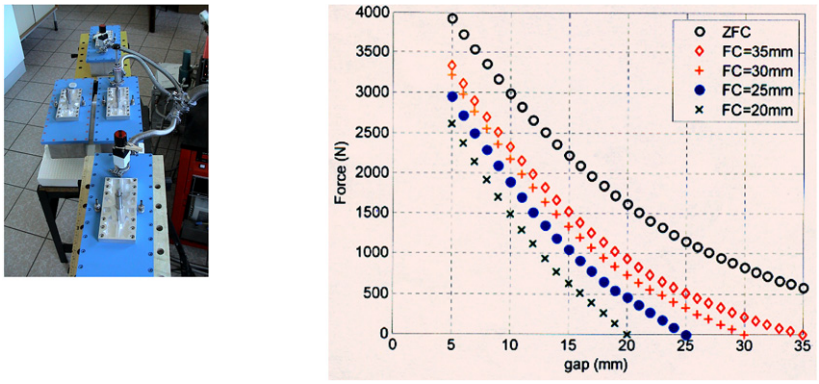

Figure 17. Maglev cryostat module in test set-up and levitation force measurement [22].

external damping systems to bring the complicated rotor dynamics under control. Three different superconducting flywheel projects and concepts are compared in view of future improvements.

The present status of magnetic levitation (Maglev) trains is examined. The magnet guideway concepts are shown to be well engineered based on FEM calculations. For the superconductor part a successful vacuum cryostat with 24 YBCO bulks and a long operational time of more than one day without refilling LN_2 is constructed by ATZ. Each cryostat can handle loads up to 2500 N@10 mm air gap on a magnet guideway. More than 30 cryostats are fabricated and being tested now in Germany, China and Brazil.

Acknowledgments

Many useful discussions with Dr Zigang Deng, presently at the Laboratory of Applied Physics, Tokyo University of Marine Science and Technology TUMSAT, Tokyo, Japan are greatly appreciated.

The intensive and fruitful cooperation with L-3 Communications Magnet-Motor GmbH, Starnberg, Germany in the field of flywheel applications is acknowledged. Part of the work was supported by the German VDI/BMBF under contract nos. 13N8737 and 13N8738.

The authors would like to thank the Maglev groups of the Applied Superconductivity Laboratory (ASCLab), Southwest Jiaotong University (SWJTU), the Laboratorio de Aplicacao de Supercondutores (LASUP), Universidade Federal do Rio de Janeiro, Rio de Janeiro, Brazil, and the IFW/EVICO Dresden Germany for valuable discussions.

References

[1] Schaetzle P, Krabbes G, Stoever G, Fuchs G and Schlaefer D 1999 Multi-seeded melt crystallization of YBCO bulk material for cryogenic applications *Supercond. Sci. Technol.* **12** 69

[2] Gruss S, Fuchs G, Krabbes G, Verges P, Stover G, Muller K-H, Fink J and Schultz L 2001 Superconducting bulk magnets: very high trapped fields and cracking *Appl. Phys. Lett.* **79** 3131

[3] Werfel F N, Floegel-Delor U, Rothfeld R, Wippich D and Riedel T 2001 Polycrystalline HTS material for bearings and electric power devices *Physica* C **357–360** 843

[4] Nariki S, Sakai N and Murakami M 2005 Melt-processed Gd–Ba–Cu–O superconductor with trapped field of 3 T at 77 K *Supercond. Sci. Technol.* **18** S126

[5] Oka T 2007 Processing and applications of bulk HTSC *Physica* C **463–465** 7

[6] Ren H, Xiao L, Jiao Y and Zheng M 2004 Processing and characterization of YBCO superconductors by top-seeded melt growth method in batch process *Physica* C **412–414** 597

[7] Nariki S, Sakai N, Kita M, Fujikura M, Murakami M and Hirabayashi I 2006 Advances in enlargement of melt-textured Gd–Ba–Cu–O superconductors *Supercond. Sci. Technol.* **19** S500

[8] Muralidhar M, Tomita M, Suzuki K, Jirsa M, Fukumoto Y and Ishihara A 2010 A low-cost batch process for high-performance melt-textured GdBaCuO pellets *Supercond. Sci. Technol.* **23** 045033

[9] Shi Y, Hari Babu N, Iida K, Yeoh W K, Dennis A R, Pathak S K and Cardwell D A 2010 Batch-processed GdBCO–Ag bulk superconductors fabricated using generic seeds with high trapped fields *Physica* C **470** 685

[10] Hull J R 2000 Superconducting bearings *Supercond. Sci. Technol.* **13** R1

[11] Koshizuka N 2006 R& Dof superconducting bearing technologies for flywheel energy storage systems *Physica* C **445–448** 1103

[12] Werfel F N, Floegel-Delor U, Riedel T, Rothfeld R, Wippich D and Goebel B 2010 HTS Magnetic bearings in prototype application *IEEE Trans. Appl. Supercond.* **20** 874

[13] Walter H, Bock J, Frohne Ch, Schippl K, May H, Canders W R, Kummeth P, Nick W and Neumueller H-W 2006 First heavy load bearing for industrial application with shaft loads up to 10 kN *J. Phys.: Conf. Ser.* **43** 995

[14] Werfel F N, Floegel-Delor U, Rothfeld R, Wippich D and Riedel T 2001 Centrifuge advances using HTS magnetic bearings *Physica* C **354** 13–7

[15] Werfel F N, Floegel-Delor U, Riedel T, Rothfeld R, Wippich D and Goebel B 2005 Encapsulated HTS bearings: technical and cost considerations *IEEE Trans. Appl. Supercond.* **15** 2306–11

[16] Ries G and Werfel F 2004 In der schwebe: supraleitende magnetlager *Phys. Z.* **35** 134–40

[17] Werfel F N, Floegel-Delor U, Riedel T, Rothfeld R, Wippich D, Goebel B, Reiner G and Wehlau N 2007 A compact HTS 5 kWh/250 kW flywheel energy storage system *IEEE Trans. Appl. Supercond.* **17** 2138

[18] Strasik M 2007 Design, fabrication, and test of a 5 kWh/100 kW flywheel energy storage utilizing a high-temperature superconducting bearing *IEEE Trans. Appl. Supercond.* **17** 2133

[19] Wang J *et al* 2002 The first man-loading high temperature superconducting Maglev test vehicle in the world *Physica* C **378–381** 809

[20] Wang S, Wang J, Ren Z, Jiang H, Zhu M, Wang X and Tang Q 2001 Levitation force of multi-block YBaCuO bulk high temperature superconductors *IEEE Trans. Appl. Supercond.* **11** 1808

[21] Schultz L, deHaas O, Verges P, Beyer C, Roehlig S, Olsen H, Kuehn L, Berger D and Noteboom Funk U 2005 Superconductively levitated transport system—the supratrans project *IEEE Trans. Appl. Supercond.* **15** 2301

[22] Sotelo G G, Dias D H, Machado O J, David E D, de Andrade R Jr, Stephan R M and Costa G C 2010 Experiments in a real scale MagLev vehicle prototype *J. Phys.: Conf. Ser.* **234** 032054

[23] Beyer C, deHaas O, Verges V and Schultz L 2006 Guideway and turnout switch for Supratrans project *J. Phys.: Conf. Ser.* **43** 991–4

[24] Jing H, Wang J, Wang S, Wang L, Liu L, Zheng J, Deng Z, Ma G, Zhang Y and Li J 2007 A two-pole Halbach permanent magnet guideway for high temperature superconducting Maglev vehicle *Physica* C **463** 426

[25] Deng Z, Wang J, Zheng J, Lin Q, Zhang Y and Wang S 2009 Maglev performance of a double-layer bulk high temperature superconductor above a permanent magnet guideway *Supercond. Sci. Technol.* **22** 055003

[26] Okano M, Iwamoto T, Senokuchi M, Fuchino S and Ishii I 2004 Magnetic rail construction for a low loss Superconducting magnetic levitation linear guide *IEEE Trans. Appl. Supercond.* **14** 944–7

[27] Dias D H N, Motta E S, Sotelo G G and de Andrade R Jr 2010 Experimental validation of field cooling simulations for linear superconducting magnetic bearings *Supercond. Sci. Technol.* **23** 075013

[28] Sotelo G G, Dias D H N, de Andrade R and Stephan R M 2011 Tests on a superconductor linear magnetic bearing of a

full-scale Maglev vehicle *IEEE Trans. Appl. Supercond.* **21** 1464–8
[29] Ikuta H 2003 *High Temperature Superconductivity Materials* ed A V Narlikar (Berlin: Springer) pp 79–97
[30] Oda M, Yao X, Yoshida Y and Ikuta H 2009 Melt-textured growth of (LRE)–Ba–Cu–O by a cold-seeding method using $SmBa_2Cu_3O_y$ thin film as a seed *Supercond. Sci. Technol.* **22** 075012
[31] Krabbes G, Bieger W, Schatzle P and Wiesner U 1998 Improved HTSC bulk materials: a thermodynamic approach to processing *Supercond. Sci. Technol.* **11** 144–8
[32] Li T Y *et al* 2010 Multiseeded melt growth of bulk Y–Ba–Cu–O using thin film seeds *J. Appl. Phys.* **108** 023914
[33] Cardwell D A *et al* 2005 Round robin tests on large grain melt processed Sm–Ba–Cu–O bulk superconductors pellets *Supercond. Sci. Technol.* **18** 173
[34] Fujishiro H, Hiyama T, Naito T, Yanagi Y and Itoh Y 2009 Enhancement of trapped filed and total trapped flux on GdBaCuO by the MMPSC + IMRA method *Supercond. Sci. Technol.* **22** 095006
[35] Deng Z, Izumi M, Miki M, Felder B, Tsuzuki K, Hara S, Uetake T, Floegel-Delor U and Werfel F N 2011 Trapped flux and levitation properties of multi-seeded YBCO bulks for HTS magnetic device applications—part I: grain and current features *IEEE Trans. Appl. Supercond.* at press
[36] Tomita M and Murakami M 2000 Improvement of the mechanical properties of bulk superconductors with resin impregnation *Supercond. Sci. Technol.* **13** 722
[37] Tomita M and Murakami M 2003 High-temperature superconductor bulk magnets that can trap magnetic fields of over 17 T at 29 K *Nature* **421** 517
[38] Floegel-Delor U, Riedel T, Wippich D, Goebel B, Rothfeld R, Schirrmeister P, Werfel F N, Usoskin A and Rutt A 2011 Reel-to-reel copper electroplating on pulse laser deposition coated conductor *IEEE Trans Appl. Supercond.* **21** 2984
[39] Hull J R and Cansiz A 1999 Vertical and lateral forces between a permanent magnet and a high-temperature superconductor *J. Appl. Phys.* **86** 6396–404
[40] Zeissberger M, Habisreuther T, Litzkendorf D, Surzhenko O, Muller R and Gawalek W 2001 Optimization of levitation forces *IEEE Trans. Appl. Supercond.* **11** 1741
[41] Arai Y, Seino H and Nagashima K 2010 Levitation properties of superconducting magnetic bearings using superconducting coils and bulk superconductors *Supercond. Sci. Technol.* **23** 115001
[42] Seino H, Nagashima K, Tanaka Y and Nakauchi M 2010 Study of superconducting magnetic bearing applicable to the flywheel energy storage system that consist of HTS-bulks and superconducting-coils *J. Phys.: Conf. Ser.* **234** 032052
[43] Werfel F N, Floegel-Delor U, Riedel T, Rothfeld R, Wippich D, Goebel B, Reiner G and Wehlau N 2010 Towards high-capacity HTS flywheel System *IEEE Trans. Appl. Supercond.* **20** 2272
[44] Hull J R, Strasik M, Mittleider J, McIver C, McCrary K, Gonder J and Johnson P 2011 Damping of sub-synchronous whirl in rotors with high-temperature superconducting bearing *IEEE Trans. Appl. Supercond.* **21** 1453–9
[45] Strasik M, Hull J R, Mittleider J, Gonder J, Johnson P, McCrary K and McIver C 2010 An overview of Boeing flywheel energy storage systems with high-temperature superconducting bearings *Supercond. Sci. Technol.* **23** 2010
[46] Koshizuka N 2010 The superconducting magnetic bearings and magnetic clutches for flywheel energy storage *PASREG' 10 (Washington, DC)*
[47] Werfel F N, Floegel-Delor U, Riedel T, Wippich D, Goebel B and Rothfeld R 2010 HTS flywheel from R&D to pilot energy storage system *J. Phys.: Conf. Ser.* **234** 032062
[48] Halbach K 1985 Application of permanent magnets in accelerators and electron storage rings *J. Appl. Phys.* **57** 3605
[49] Schultz L 2011 *EUCAS (den Haag, Sept.)* www.evico.de